Title: Analysis of caspase-mediated suppression of the cGAS/STING pathway in Kaposi's sarcoma-associated herpesvirus lytic infection reveals a dramatic cellular heterogeneity in type I interferon responses

Authors: Tate Tabtieng[1,2,5,6], Rachel C. Lent[1,3,6], Alvaro Monago Sanchez[1,4], Marta Maria Gaglia[1,2,3]

[1] Department of Molecular Biology and Microbiology, Tufts University School of Medicine, Boston, MA

[2] Program in Biochemistry, Tufts University Graduate School of Biomedical Sciences, Boston, MA

[3] Program in Molecular Microbiology, Tufts University Graduate School of Biomedical Sciences, Boston, MA

[4] Faculty of Experimental Sciences, Universidad Francisco de Vitoria, Madrid, Spain

[5] Present address: Generate Biomedicines, Cambridge, MA

[6]These authors contributed equally

Correspondence to: Marta Maria Gaglia, Marta.Gaglia@tufts.edu

Abstract

As a result of the ongoing virus-host arms race, viruses have evolved numerous immune subversion strategies, many of which are aimed at suppressing the production of type I interferons (IFNs)[1]. This focus on IFN evasion highlights the essential role of these cytokines in controlling viral infections. Apoptotic caspases have recently emerged as important regulators of type I IFN signaling in both non-infectious contexts and during viral infection[2–5]. Despite being widely considered anti-viral factors since they can trigger cell death, several apoptotic caspases promote viral replication by suppressing innate immune responses[2–5]. Indeed, we previously discovered that the AIDS-associated oncogenic gammaherpesvirus Kaposi's sarcoma-associated herpesvirus (KSHV) exploits caspase-8 activity to suppress the antiviral type I IFN response and promote viral replication[5]. However, the mechanism of this novel viral immune evasion strategy is poorly understood, particularly how caspase-8 antagonizes IFN signaling during KSHV infection. Here we show that caspase activity inhibits the DNA sensor cGAS[6] during KSHV lytic replication to block type I IFN induction. Furthermore, we use single-cell RNA-sequencing to reveal that the potent antiviral state conferred upon caspase inhibition is mediated by an exceptionally small percentage of IFN-β-producing cells, thus uncovering further complexity of IFN regulation during viral infection. Collectively, these results provide insight into multiple levels of cellular type I IFN regulation that viruses co-opt for immune evasion. Unraveling these mechanisms can inform targeted therapeutic strategies for viral infections and reveal cellular mechanisms of regulating interferon signaling in the context of cancer and chronic inflammatory diseases.

Upon infection of a host cell, viral nucleic acids are sensed by cellular pattern recognition receptors such as the cytosolic DNA sensor cGAS and RNA sensor RIG-I[7]. These sensors signal through adaptor proteins (STING and MAVS, respectively) and the kinases TBK1 and IKKε to activate the transcription factor IRF3 and trigger induction of type I IFN cytokines[7]. Type I IFNs in turn stimulate expression of interferon stimulated genes (ISGs) in an autocrine and paracrine manner to limit viral replication and infection[8]. As ISGs create a strong antiviral response, all viruses have evolved one or more strategies to block IFN induction[1]. Indeed, KSHV induces minimal type I IFN responses when reactivating from latency[5,9], demonstrating it can strongly block this response. While many viral encoded factors directly target the type I IFN response, viruses have also evolved strategies to usurp cellular pathways to counteract immune responses. Although apoptotic caspases are canonically thought to be antiviral by facilitating cell death of infected cells, recent studies have demonstrated caspase-dependent inhibition of innate immune signaling during apoptosis and viral infection[2–5]. Caspase-3 and -7 can directly cleave cGAS, MAVS, and IRF3 to block type I IFN signaling[4]. In addition, we established that KSHV exploits caspase-8 activity to suppress the type I IFN response, independently of caspase-3/7 activation[5]. Indeed, while KSHV lytic reactivation normally does not induce a strong type I IFN response, lytically infected cells express and secrete high levels of IFN-β if caspase-8 (but not caspase-3/7) is inhibited[5]. KSHV uses this mechanism to promote viral replication while at the same time preventing caspase-mediated cell death[5]. However, it is unclear how caspase-8 enacts this IFN regulatory function.

We previously showed that the type I IFN response that occurs upon caspase inhibition is dependent on the kinase TBK1[5]. TBK1 can be activated by several pathogen sensors, including sensors of viral nucleic acids[7]. To discern which pathogen sensing pathway is inhibited by

caspase activity during KSHV infection, we knocked down key proteins for DNA and RNA sensing: the DNA sensors cGAS and IFI16 and their signaling adaptor STING, and the RNA sensor RIG-I and its signaling adaptor MAVS (Fig. 1A-C, Supp Fig. 1). Both the DNA and the RNA sensing pathways can be activated during KSHV infection[9–16]. For these experiments, we used iSLK.219 cells, which are latently infected with recombinant rKSHV.219. rKSHV.219 expresses GFP constitutively and RFP under the control of a KSHV lytic promoter[17]. These cells also express an exogenous copy of the KSHV master lytic regulator RTA under a doxycycline inducible promoter, so that reactivation of the viral lytic replication cycle can be induced by doxycycline treatment[17]. IFN-β induction upon caspase inhibition was severely reduced by STING and cGAS depletion, suggesting that caspase activity targets STING-dependent type I IFN signaling during KSHV replication (Fig. 1A). Moreover, upon STING and cGAS knock-down, caspase inhibitors no longer caused a reduction in KSHV replication, which we previously showed is a result of type I IFN induction[5] (Fig.1B). In contrast, IFI16, RIG-I, and MAVS knockdowns had minimal effects on IFN-β induction and viral gene expression in the presence of caspase inhibitors (Fig. 1A, B). These results suggest that cGAS/STING-mediated DNA sensing in particular is disabled by caspase activity. To corroborate this conclusion, we also tested pharmacological inhibition of cGAS enzymatic activity with RU.521. When bound to DNA, cGAS synthesizes the cyclic dinucleotide 2'3'-cGAMP, which in turn binds and activates STING[18]. Consistent with our knock-down results, cGAS inhibition reduced induction of IFN-β (Fig. 1D) and of the interferon-stimulated gene ISG15 (Supp. Fig. 2A) upon caspase inhibition. Collectively, these findings suggest that caspase activity prevents activation or signal transduction of the cGAS/STING DNA sensing pathway during KSHV lytic replication.

Figure 1

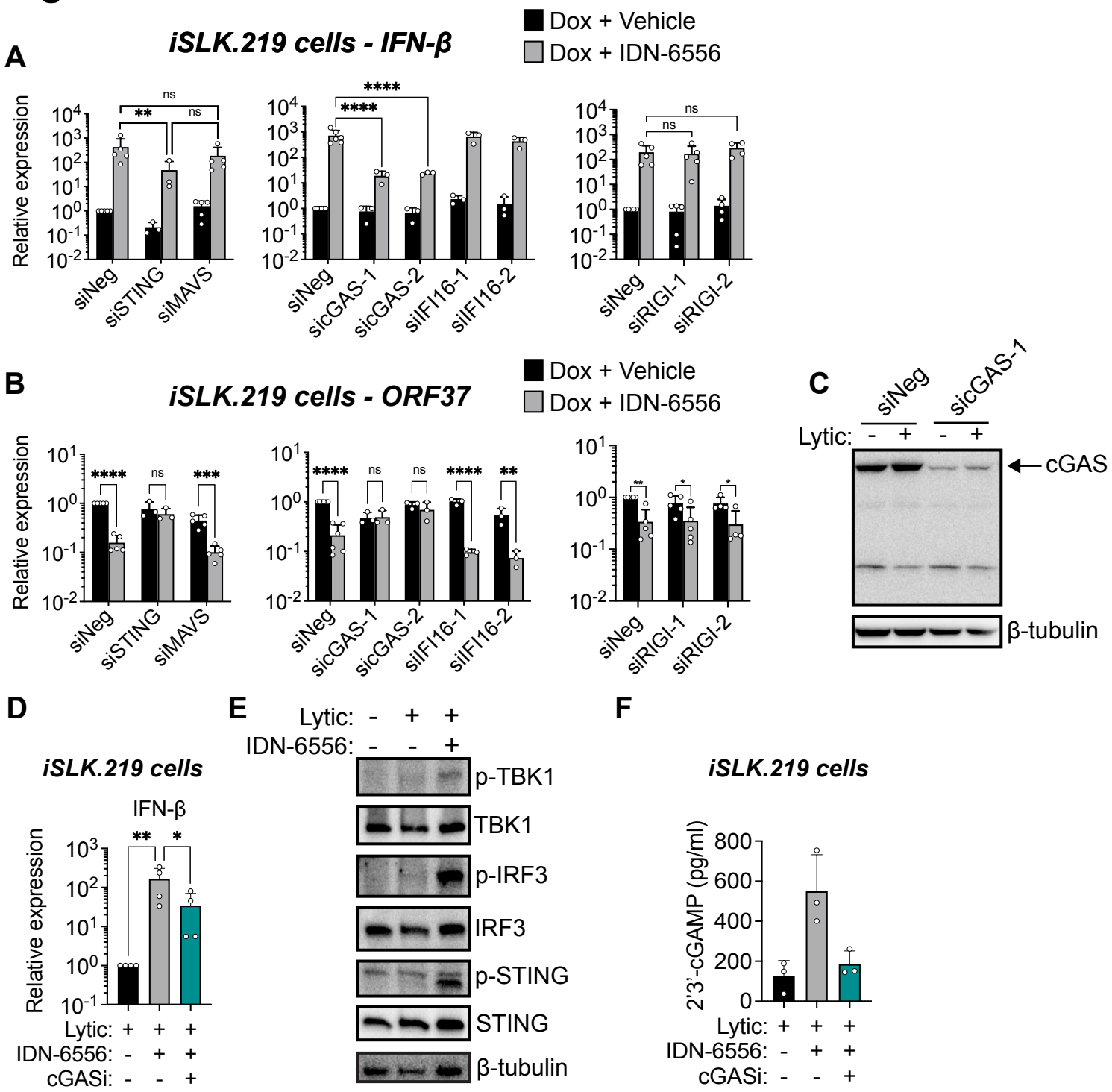

Figure 1. Caspase activity prevents cGAS activation during KSHV lytic replication to block IFN-β induction

(A-C) iSLK.219 cells were transfected with a negative control siRNA or siRNAs targeting the indicated proteins. For cGAS and RIG-I, the transfection was carried out twice, two days prior to and on the day of lytic cycle induction; for STING, MAVS and IFI16, one transfection was carried out two days prior to induction. The cells were then lytically reactivated with doxycycline (1 μg/ml) and treated with either DMSO (vehicle) and IDN-6556 (10 μM) as indicated. (A-B) Total RNA was extracted at day 5 post reactivation and the levels of IFN-β (A) and ORF37 (B) mRNA were measured by RT-qPCR and normalized to levels of 18S rRNA ($n \geq 3$). (C) Cell lysates were harvested at day 4 post reactivation and subjected to western blot for cGAS and β-tubulin as a loading control. Blots are representative of 3 replicates. (D-F) iSLK.219 cells were lytically reactivated with doxycycline (1 μg/ml) and treated with either DMSO (vehicle) or IDN-6556 (10 μM) and the cGAS inhibitor RU.521 (cGASi, 24.1 μM), where indicated. (D) Total RNA was extracted from iSLK.219 cells 3 days after reactivation. Levels of IFN-β mRNA were measured by RT-qPCR and normalized to 18S rRNA ($n = 3$). (E) Cell lysates were harvested at day 4 post reactivation and subjected to western blotting for p-TBK-1, TBK-1, p-IRF-3, IRF-3, p-STING, STING, and β-tubulin (as a loading control) as indicated. Blots are representative of 3 replicates. (F) Levels of 2'3'-cGAMP in lysate collected from iSLK.219 cells at day 4 post reactivation were measured by ELISA ($n = 4$). ns, *, **, ***, ****: p value > 0.05, < 0.05, < 0.01, < 0.001, < 0.0001, Tukey's multiple comparisons test after two-way ANOVA.

To determine how caspases interfere with cGAS/STING signaling, we tested whether there was differential activation of various effectors in the cGAS/STING pathway in the presence *vs*. absence of caspase activity. We observed increased phosphorylation of the downstream proteins STING, TBK1, and IRF3, which indicates that they are activated upon caspase inhibition (Fig.1E). These results suggest that activation of the entire pathway is blocked by caspases. Indeed, we also found that 2'3'-cGAMP levels were increased upon caspase inhibition and were reduced by treatment with a cGAS inhibitor (Fig.1F). Taken together with our results from the knockdown experiments, these findings identify the target of caspases as a component or regulator of the cGAS/STING pathway that acts to promote activation or activity of cGAS.

We considered the possibility that the target was cGAS itself. One report suggests that caspase-3 and -7 can cleave cGAS during apoptosis and other viral infections[4]. However, we have found that the activity of these caspases is dispensable for IFN regulation during KSHV lytic infection, and that caspase-8 is the key regulator[5]. Indeed, we do not detect an overall reduction in cGAS levels nor any cGAS cleavage fragments during lytic reactivation (Fig. 1C). Ectopic co-expression of caspase-8 and cGAS also does not reveal caspase degradation fragments, even though caspase-8 overexpression also activates caspase-3 and -7 (data not shown). It is thus likely that during KSHV lytic infection, caspase-8 inhibits cGAS by targeting a key regulatory factor that modulates its activity.

To determine if caspases also suppress the cGAS/STING pathway in a cell type that is physiologically relevant for KSHV infection and tumorigenesis, we examined the activity of caspases in BC3 cells, a KSHV-infected B cell line derived from a primary effusion lymphoma

(PEL) patient[19]. Caspase-8 was also activated upon lytic reactivation of BC3 cells (Fig. 2A). Moreover, caspase inhibition increased expression of both IFN-β and ISGs (ISG15 and IFIT1, Fig. 2B), as well as IRF3 phosphorylation (Fig. 2C). Consistent with what we observed in iSLK.219 cells, caspase inhibition potentiated 2'3'-cGAMP production in lytically reactivated BC3 cells (Fig. 2D). Moreover, inhibition of cGAS with RU.521 reduced the induction of IFN-β (Fig. 2E) and, to some extent, ISG15 (Supp Fig.2B). These results strengthen our conclusion that caspases have a major role in inhibiting cGAS activity or activation to block IFN induction during KSHV lytic infection.

These results provide a bulk analysis of the IFN pathway during KSHV infection. However, not all iSLK.219 cells in the population re-enter the lytic cycle upon doxycycline addition[17], suggesting there could be significant cell-to-cell variability in responses to infection. To understand both lytic reactivation and IFN signaling on a single cell basis, we carried out single-cell RNA sequencing (scRNAseq) on uninfected cells, latently infected cells, lytically infected cells, and lytically infected cells treated with IDN-6556 (Fig. 3A, Table S1). Uninfected cells are SLK cells containing the inducible KSHV RTA transgene, but no rKSHV.219[17]. We also included lytically infected cells treated with IDN-6556 and anti-IFN antibodies to block autocrine and paracrine signals (Fig. 3A, Supp. Fig. 3A, Table S1). Analysis using the Seurat package[20,21] unbiasedly identified 13 clusters with different gene expression across the 4 samples (Fig. 3B). Analysis of the mapped reads showed that, as expected, there was a higher percentage of KSHV reads in cells that were lytically reactivated (Fig. 3C, D). Certain clusters were clearly enriched in KSHV transcripts (Fig.3C, E; Supp. Fig. 3B) and these corresponded to clusters that only appeared in the lytic samples (Fig. 3B, C). Analysis of the cell cycle status indicated that most of the cells were in G1, but some of the clusters were enriched in cells in S or G2/M phase,

Figure 2

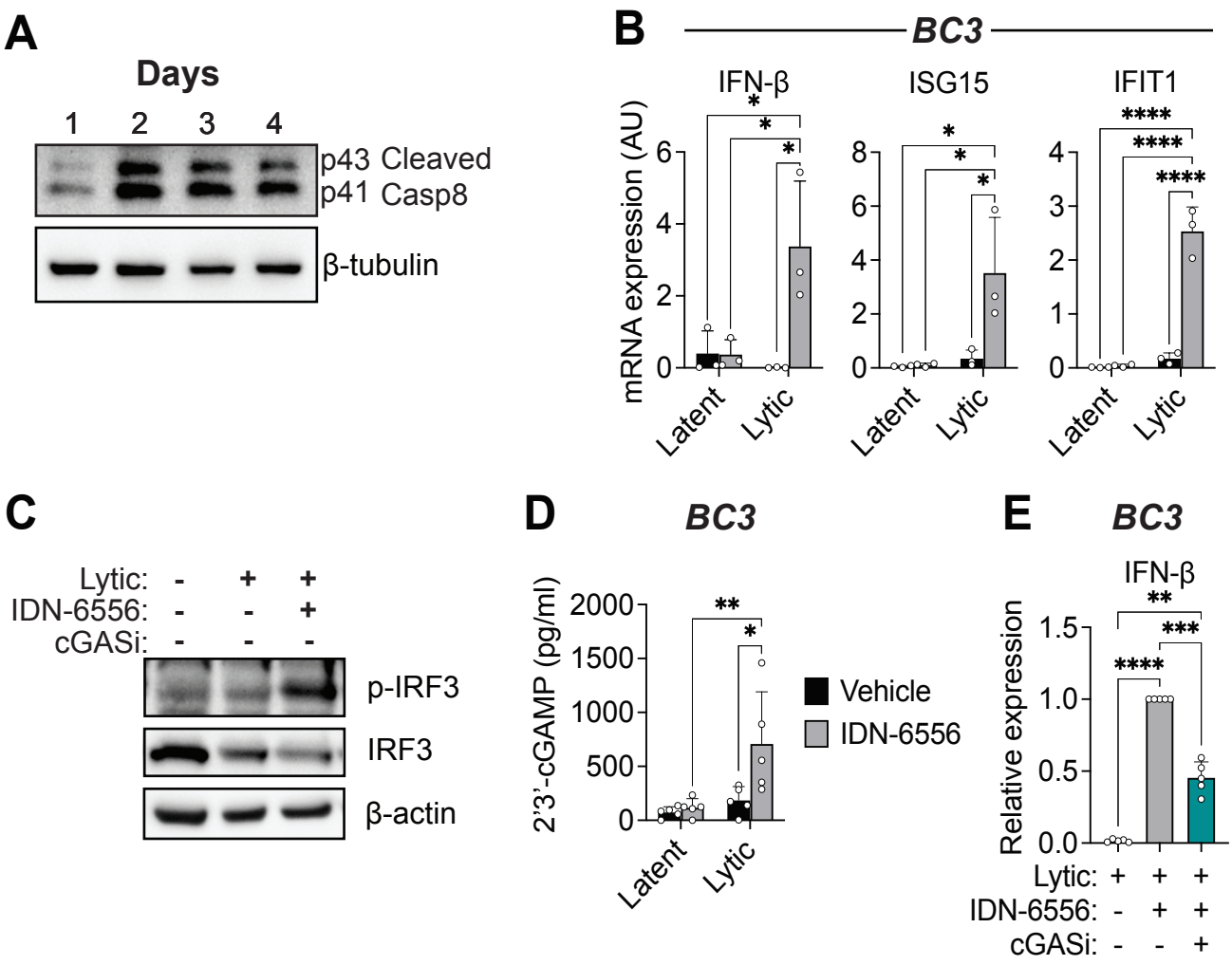

Figure 2. Caspases also inhibit cGAS activity in KSHV infected B cells

BC3 cells were lytically reactivated with TPA (20 ng/ml) for 1-3 days as indicated (A) or for 2 days (B-E) and treated with DMSO (vehicle), the pan-caspase inhibitor IDN-6556 (10 μM), and/or the cGAS inhibitor RU.521 (cGASi, 24.1 μM) as indicated. (A) Cell lysates were collected from latent and lytically reactivated BC3 cells at the indicated time points and subjected to western blot analysis for activated (cleaved) caspase-8, and β-tubulin as a loading control. Blots are representative of 3 replicates. (B) Total RNA was extracted from BC3 cells. Levels of the indicated mRNAs were measured by RT-qPCR and normalized to 18S rRNA (n = 3). (C) Cell lysates were collected from lytically reactivated BC3 cells and subjected to western blot analysis for activated p-IRF3, total IRF3, and β-actin as a loading control. Blots are representative of 3 replicates. (D) Levels of 2'3'-cGAMP in lysate collected from BC3 were measured by ELISA (n = 5). (D) Total RNA was extracted from BC3 cells. Levels of IFN-β mRNA were measured by RT-qPCR and normalized to 18S rRNA (n = 5). *, **,***,****: *p* value < 0.05, < 0.01, < 0.001, < 0.0001, Tukey's multiple comparisons test after two-way ANOVA.

Figure 3

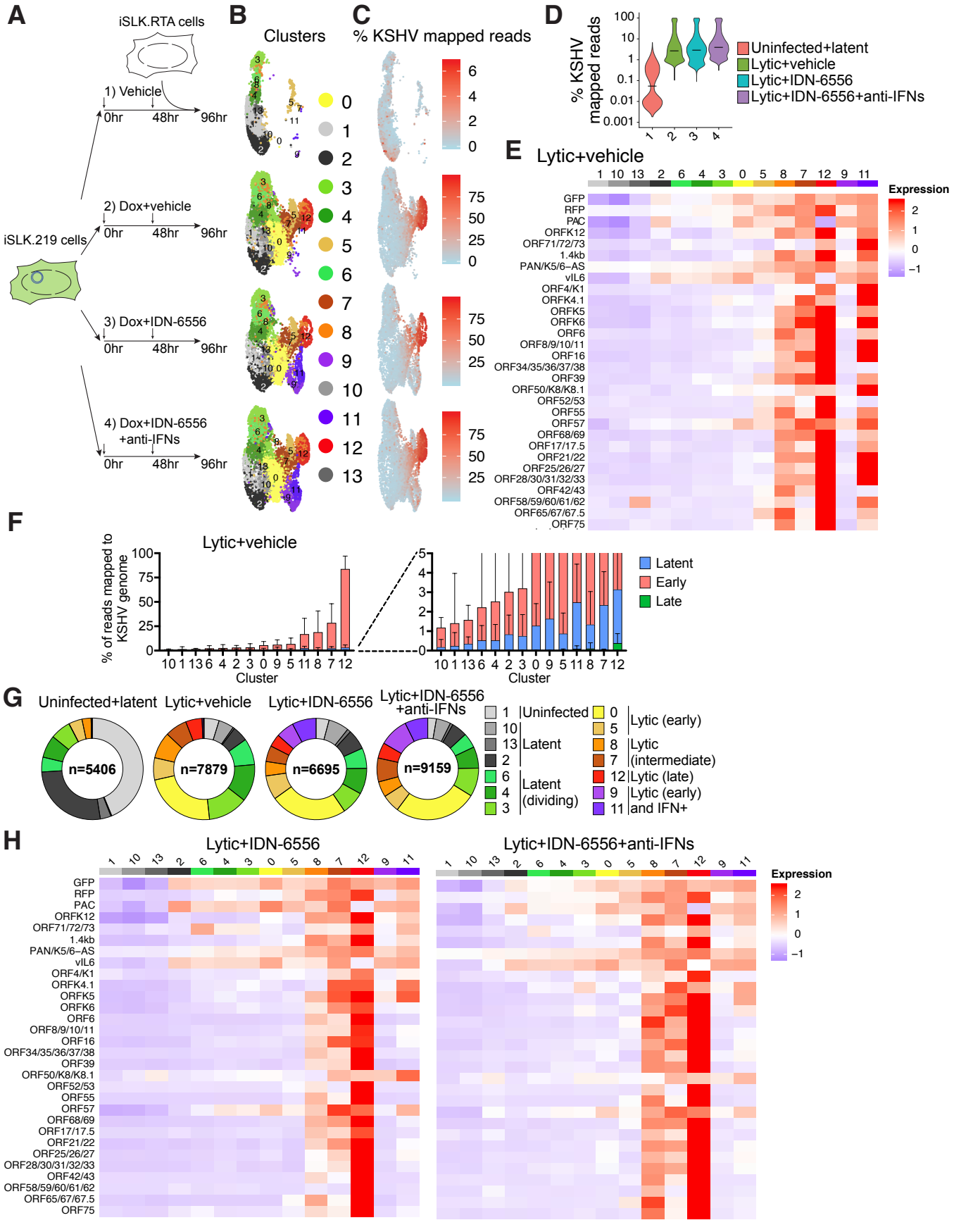

Figure 3. Single-cell RNAseq analysis reveals subsets of lytically reactivating cells. (A) Diagram of the single-cell RNAseq (scRNAseq) experiment using 4 samples. Sample 1 was a mixture of uninfected iSLK.RTA and latently infected iSLK.219 cells treated with DMSO (vehicle). Samples 2-4 were iSLK.219 treated with doxycycline (Dox) to reactivate lytic replication ("Lytic") and treated with DMSO (vehicle), the caspase inhibitor IDN-6556, or IDN-6556 and a cocktail of anti-IFN antibodies to block paracrine IFN signaling. All samples were collected 4 days after the start of treatments. (B-H) Analysis of data from the scRNAseq experiment presented in (A). (B) UMAP diagram of the clusters unbiasedly defined by Seurat in the 4 samples. (C) UMAP diagram showing what percentage of reads from each cell comes from the KSHV genome. Legends on the right define what percentage the colors represent. (D) Violin plot of the distribution of cells in each sample based on percentage of KSHV reads. Sample 1 has a bimodal distribution because it is a mix of uninfected and latent cells. (E) Heatmap of average expression of KSHV genes in each cluster in the lytic + vehicle sample. The legends on the right define what expression level the colors represent (arbitrary units). Corresponding heatmap with gene expression in each individual cell can be found in Supp. Fig. S3B. (F) Plot of percentage reads per cell that map to each of three types of KSHV genes (latent, early and late) in each cluster in the lytic + vehicle sample. Clusters are sorted based on the total average percentage of KSHV reads. (G) Pie-charts of percentage of cells that map to each cluster in the four samples. (H) Heatmap of average expression of KSHV genes in each cluster in the lytic + IDN-6556 and lytic + IDN-6556 + anti-IFN samples. The legends on the right define what expression level the colors represent (arbitrary units). Corresponding heatmaps with gene expression in each individual cell can be found in Supp. Fig. S3B.

and this tended to correlate with lower viral gene expression, presumably indicative of lower reactivation (Supp. Fig. 3C). We further analyzed the type of genes that were seen in the different clusters in the lytic+vehicle sample, and saw that only cells in cluster 12 appeared to have more than 25% KSHV reads on average (Fig. 3E-F, Supp. Fig 3B). Because our scRNAseq is directed at the 3' end of RNAs and many mRNAs in KSHV have the same 3' end[22,23], we were not able to conclusively distinguish expression of all the viral genes. Therefore, in the heatmaps we list together all the ORFs that each 3' end corresponds to. Nonetheless, analysis of viral genes and of the rKSHV.219-encoded GFP, RFP and puromycin-N-acetyl transferase (PAC) reporters agrees with the general picture obtained from percentage reads. Most clusters show some lytic gene expression but only a few demonstrate substantial expression of lytic genes (Fig. 3E, Supp. Fig. 3B). Interestingly, we note that some of the clusters that expressed lytic genes did not express high levels of RFP (cluster 0 for example, Fig. 3E). Because KSHV lytic genes are expressed in several waves, termed early lytic, delayed early and late[24–26], we roughly categorized the clusters based on the pattern of lytic gene expression, as well as the cell cycle stage and the expression of IFNs. We classified clusters as "uninfected", "latent", "latent (dividing)", "lytic (early)", "lytic (intermediate)", "lytic (late)", "lytic (early) and IFN+" (Fig. 3E, 3G-H, Fig. 4A-C). Most of the viral transcripts detected increased in levels monotonically in cells that had progressed further through the lytic cycle, except for ORF57, K4.1, and vIL-6, which appeared to decrease in levels in the "late" lytic cell cluster (cluster 12, Figure 3E). Figure 3G and Supp. Fig. 3B show how the different clusters expanded and contracted in each sample. Interestingly, addition of the caspase inhibitors and the consequent type I IFN induction did not reduce the overall percentage of cells expressing lytic genes (Fig. 3G, Table S2), but it reduced the number of cells that we classified as "lytic (intermediate)" and "lytic (late)" (particularly

clusters 7 and 12) and the levels of viral genes in the "lytic (intermediate)" clusters (clusters 8 and 7) (Fig. 3E, G, H, Supp. Fig. 3B). The effect of caspase inhibitors on the size of these clusters and the reduction in lytic gene expression in clusters 8 and 7 was largely rescued by blocking type I IFN signaling with anti-IFN antibodies (Fig. 3G, H, Supp. Fig. 3B). These results confirm that caspase activity is required for reactivation and/or progression through the lytic cycle and that inhibition of the lytic cycle upon caspase inhibition is due to the paracrine and autocrine effects of type I IFN secretion. They thus recapitulate our bulk level findings on the role of caspases during KSHV replications[5]. The scRNAseq results also confirm the wide variability in stage of reactivation of iSLK.219 cells and reveal that the RFP signal in iSLK.219 cells may underestimate the cells that are expressing lytic genes.

An outstanding question from our bulk analysis was the identity of the cells that produce IFN-β in the caspase inhibitor-treated samples. We hypothesized that the lytically reactivating cells, rather than the latent ones, produce IFNs, and our scRNAseq data showed that type I IFN expression is indeed limited to cells that express viral lytic genes (Fig. 3H). However, the scRNAseq also surprising revealed that only 3.8% of the cells in the caspase inhibitor-treated samples expressed IFNs, particularly IFN-β (Fig. 4B). The IFN-β+ cells were concentrated in clusters 9 and 11, which only appeared in the +IDN-6556 samples (Fig. 4A, B). We did not detect expression of IFN-αs, but we saw that cells in these clusters also expressed the type III IFN IFN-λ1 (Fig. 4C, Supp Fig 4A). Nonetheless, the IFN coming from this small fraction of cells was sufficient to elicit a strong response in the entire population of cells, as indicated by the IFN-dependent increase in expression of interferon stimulated genes (ISGs) after IDN-6556 treatment across almost all clusters (Fig. 4D, E, Supp. Fig. 4B). Moreover, as we previously showed in bulk analysis, type I IFN signaling reduced viral gene expression across the

Figure 4

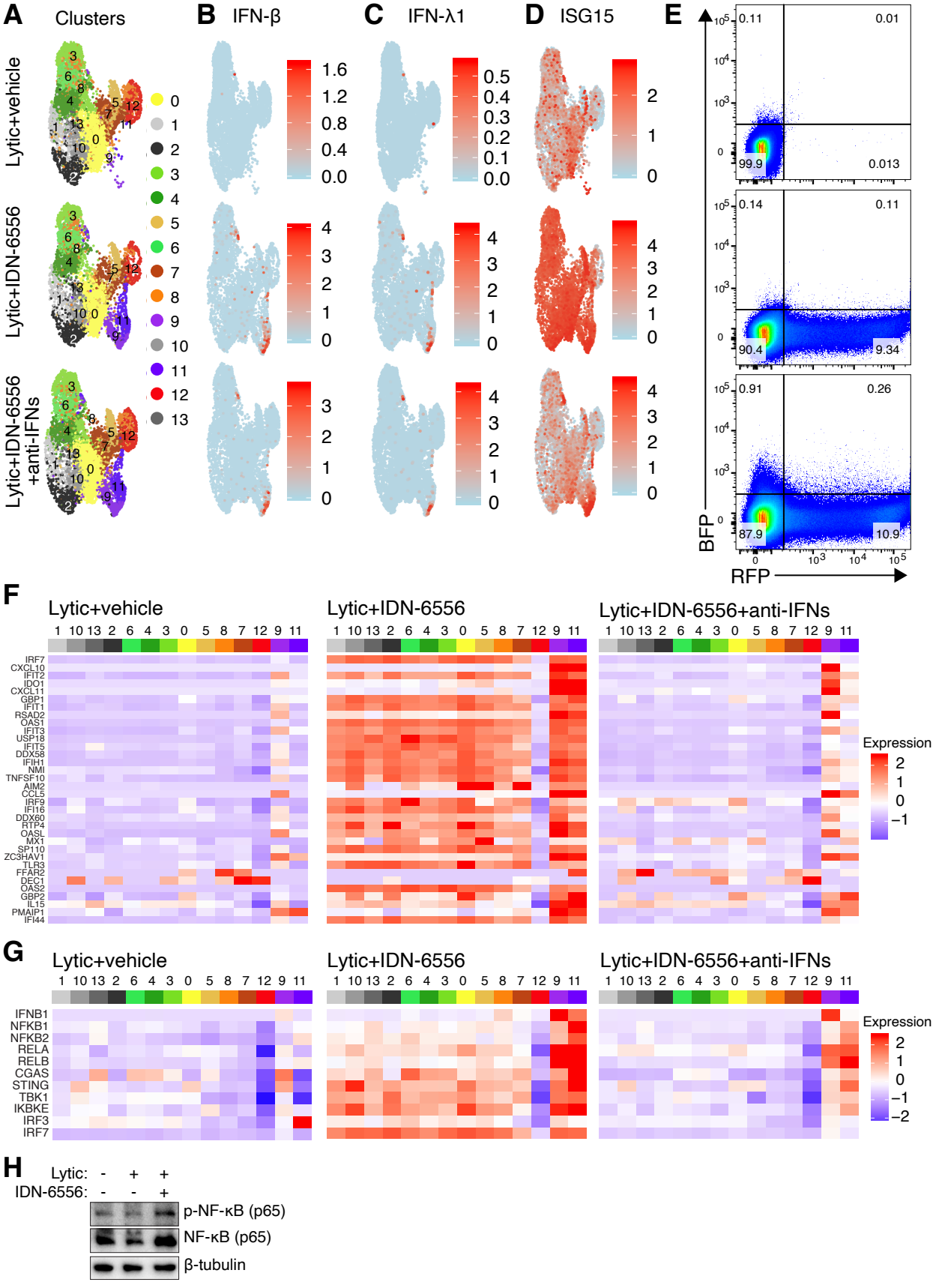

Figure 4. Only a small fraction of KSHV lytic cells express IFN-β. (A-D) Analysis of data from the scRNAseq experiment presented in Fig. 3A. (A) UMAP diagram of the clusters unbiasedly defined by Seurat in the 3 lytic samples (same as Fig. 3B). (B-D) UMAP diagram of the level of expression of IFN-β (B), IFN-λ1 (C) or ISG15 (D) in each cell for the 3 lytic samples. The legends on the right define what expression level the colors represent (arbitrary units). (E) iSLK.219 expressing TagBFP from a human IFN-β promoter were treated with doxycycline to reactivate the lytic cycle ("lytic") and IDN-6556, where indicated. Flow cytometry was carried out on the cells 4 days after doxycycline addition. RFP axis reflects the RFP signal in lytic cells and BFP axis reflects activity of the IFN-β promoter. Percentage of cells mapping to each quadrant are listed. Flow cytometry plots are representative of 3 repeats. (F-G) Analysis of data from the scRNAseq experiment presented in Fig. 3A. Heat maps of average expression of ISGs (F) or select genes from the type I IFN induction pathway (G) in each cluster for the three lytic samples. The legends on the right define what expression level the colors represent (arbitrary units). Corresponding heatmaps with gene expression in each individual cell can be found in Supp. Fig. S4B. (H) iSLK.219 were treated with doxycycline to reactivate the lytic cycle ("lytic") and with IDN-6556 where indicated. Protein lysates were collected at day 4 and analyzed by western blotting for NF-κB, phospho-NF-κB (p-NF-κB) and β-tubulin as a loading control. Blots are representative of 3 replicates.

population (Fig. 3C, E, H). To ensure that the variability in IFN-β induction is not an artifact of a limit of detection by scRNAseq we constructed a cell line that expresses the TagBFP protein under the control of the IFN-β promoter. When the lytic cycle was induced in these cells concomitantly with caspase inhibitor treatment, we found that ~1% of the cells became TagBFP+ (Fig. 4E). The percentage was similar among RFP positive and negative cells, which is consistent with our scRNAseq results. Overall, these data show that an exceedingly small fraction of cells induce IFNs even under caspase inhibition, yet they can elicit a strong anti-viral response in the entire cell population.

We considered the possibility that only a subset of cells makes IFN-β due to differential expression of viral genes. For example, IFN-β+ cells could lack expression of KSHV-encoded anti-IFN factors. Consistent with this idea, cells in the IFN-β+ clusters expressed only early lytic genes and low levels of the RFP lytic marker (Fig. 3H, Supp. Fig S3B, clusters 9 and 11). However, their expression pattern was similar to that of other clusters that do not express IFNs, especially cluster 0 (Fig. 3H, Supp. Fig S3B), suggesting that differential expression of viral genes does not explain the restricted IFN-β expression pattern. Another possibility is that IFN-β+ cells express higher basal levels of genes in the type I IFN induction pathway and are thus more sensitive to IFN-inducing cues. This model was proposed in the case of other viral infections by Zhao *et al.*[27]. Analyzing these genes is complicated by the fact that many of them are themselves ISGs. Indeed, their expression was increased by type I IFN signaling in the caspase inhibitor-treated samples and was reduced back to basal levels by anti-IFN antibody treatment (Fig. 4G, Supp. Fig. 4B). Nonetheless, there was a clear enrichment of transcripts for the NF-κB transcription factor family members (NFKB1, NFKB2, RELA, RELB) in the IFN-β+ clusters 9 and 11 (Fig. 4G, Supp. Fig. 4B). NF-κB is also needed for IFN-β transcription downstream of

pathogen sensors, together with IRF3[7]. Indeed, levels and phosphorylation of NF-κB were increased in lytic cells treated with IDN-6556, showing that caspase activity also modulates NF-κB activation (Fig. 4H). It is thus possible that high NF-κB expression is needed to induce type I IFN in these cells, perhaps as a feed-forward mechanism to ensure commitment to IFN production.

This study provides mechanistic insights into multiple levels of type I IFN regulation during KSHV infection. The cGAS/STING pathway has emerged in recent years as a crucial component of the innate immune response to DNA viruses and various other pathogens[6]. This is highlighted by the multitude of strategies employed by pathogens[28], including herpesviruses[29], to disrupt the cGAS/STING pathway. While this immunosuppression is often driven by virus-encoded proteins, we have uncovered an intriguing mechanism in KSHV infection, which involves the hijacking of a host cell component, caspase-8[5], to subvert immune activation and viral clearance. While caspase-3 and -7 have been reported to directly cleave cGAS in an apoptotic setting and some viral infections[4], caspase-8 activity mediates type I IFN suppression in KSHV-infected cells without triggering apoptosis, and caspase-3 activity is dispensable[5]. These observations, in conjunction with the current study, suggest an unexpected type I IFN regulatory function of caspase-8 activity in targeting the cGAS/STING pathway that is separate from its apoptotic activity. Caspase-8 is an attractive therapeutic target that could be exploited to potentiate cGAS/STING-mediated immune responses for viral clearance. This could have far reaching implications for other pathologies, as regulation of the cGAS/STING pathway is fundamental in various inflammatory diseases and in tumor immunity[30,31], and thus is a current focus of intensive drug discovery research efforts.

The notable cellular heterogeneity in type I IFN production reveals an additional layer of complexity and regulation of innate immune responses during KSHV infection. We detect an exceptionally small fraction of IFN-β+ cells upon caspase inhibitor treatment (< 5%, Fig. 4B). Remarkably, this small IFN-β+ cell population still induces a robust IFN response in the population (Fig. 4D, F). On a practical level, the high heterogeneity in IFN-β expression complicates our analysis of caspase-8 regulation of cGAS. It is possible that the upstream portions of the pathway (i.e. cGAS) are also only active in the IFN-β+ cells, and that cell sorting may be needed to detect differences in the levels of the direct target(s) of caspase-8 in IFN regulation. Alternatively, it is possible that only a subset of the cells in which the IFN induction pathway is activated end up expressing IFN-β. In support of this idea, we were able to easily detect phosphorylation of many of the components of the IFN induction pathway using bulk analysis (Figs. 1E, 2C, 4H).

Other studies have also showed that only a small number of cells respond to infection in a population during infection with a number of other viruses[27,32–37]. Interestingly, several of these studies investigated infections in immune cell types and fibroblasts and saw higher percentages of responding cells (10-30%)[27,32,33]. In contrast, iSLK.219 cells are of epithelial origin[38]. Epithelial cells are often the first exposed to invading pathogens and mount responses that alert and prime surrounding cells to counteract viral spread. Therefore, it is possible that epithelial cell responses are even more tightly regulated to prevent inadvertent activation of the pathway. Consistent with this idea, influenza A virus and SARS coronavirus 2 infection of epithelial cells also elicit responses in a small minority of cells[34–36].

It is unclear what the source of the heterogeneity is in KSHV-infected cells. Viral gene expression, and in particular in viral immune regulators, is often considered the reason for limited type I IFN responses[36]. However, we find that IFN-β+ cells have a similar expression pattern as cells that do not make IFNs (Fig. 3E, H, Supp. Fig. 3B). While we cannot exclude the possibility that one specific gene is responsible for the difference, especially since we do not reliably detect all viral genes, these results suggest that inherent differences in the cells govern the heterogeneity. Stochasticity in gene expression, which is common among cytokines, has also been proposed as driver of type I IFN expression heterogeneity. Zhao *et al*. suggested some of this stochasticity may be epigenetically encoded[27], reducing the number of cells that are able to express type I IFN, perhaps to prevent over-activation and inflammation. Paracrine IFN signaling is also thought to influence and modulate heterogeneity[37]. This cell-cell communication may fine tune immune signal amplification in a cell density-dependent manner. Indeed, we observe 3.8% IFN-β+ cells in the IDN-6556 treated sample, but only 1.6% IFN-β+ cells in the sample treated with IDN-6556 and anti-IFN antibodies that block IFN signaling. Moreover, while cells in cluster 9 retain high average IFN-β expression even when IFN signaling is blocked, cluster 11 cells have lower IFN-β under these conditions (Fig. 4G, Supp. Fig. 4A,B), suggesting two different modes of IFN induction in these groups of cells. This reinforces the notion of self-amplification of the type I IFN response as a layer of regulation that directs selective robust responses in appropriate contexts for infection control, while avoiding tissue damage from unnecessary inflammation.

Methods

Cell lines, reagents, and treatments

All cells were cultured at 37 °C and 5% CO_2 conditions. iSLK.219, iSLK.219-IFNBp-BFP, iSLK.RTA[17], and HEK293T cells were grown in Dulbecco's modified Eagle's medium (DMEM; Life Technologies) supplemented with 10% fetal bovine serum (FBS) (HyClone). BC3 cells were grown in RPMI supplemented with 20% FBS, 2 mM GlutaMAX supplement, and 50 μM β-mercaptoethanol (Gibco/Thermo Fisher). iSLK.219 cells were reactivated with 1 μg/ml of doxycycline (Thermo Fisher). Reactivation was confirmed visually for all iSLK.219 samples by examining the appearance of RFP-positive cells (RFP is driven by the lytic PAN promoter). BC3 cells were reactivated with 20 ng/ml of TPA for 48 h. iSLK.219-IFNBp-BFP cells were generated by transducing iSLK.219 cells with lentiviruses containing pJP1_IFNBp-tagBFP. This construct is based on pLJM1-GFP, a gift from David Sabatini (Addgene plasmid # 19319 ; http://n2t.net/addgene:19319 ; RRID:Addgene_19319)[39]. The CMV promoter in this plasmid was replaced with a human IFN-β promoter subcloned from a luciferase reporter construct (kind gift of Michaela Gack) and the GFP sequence was replaced with a TagBFP sequence. In addition, the antibiotic resistance gene was changed from a puromycin resistance to a zeocin resistance gene. Lentiviral packaging was carried out using packaging plasmids pMDLg/pRRE (Addgene plasmid # 12251 ; http://n2t.net/addgene:12251 ; RRID:Addgene_12251), Addgene plasmid # 12253 ; http://n2t.net/addgene:12253 ; RRID:Addgene_12253) and pMD2.G (Addgene plasmid # 12259 ; http://n2t.net/addgene:12259 ; RRID:Addgene_12259), kind gifts

from Didier Trono[40]. Where indicated, cells were treated with vehicle (dimethyl sulfoxide [DMSO]; Sigma-Aldrich), 10 μM IDN-6556 (MedChem Express or Selleck Chemicals), 24.1 μM RU.521 (Invivogen), 1:50, 1:100, or 1:500 dilutions of a mixture of neutralizing antibodies against type I IFNs (PBL Assay Science, catalog # 39000-1). The concentrations of all drug treatments were chosen based on common concentrations used in previously published studies.

siRNA knockdown

iSLK.219 cells were transfected while in suspension (reverse transfection) with 10 nM siRNAs (purchased from Thermo Fisher) against STING (HSS139156), MAVS (HSS148537), cGAS (siRNA#1, HSS132955; siRNA#2, HSS132956), IFI16 (siRNA#1, HSS105205; siRNA#2, HSS105206), RIG-I (siRNA #1, s24144; siRNA #2, s223615), or a nontargeting siRNA (12935300) at a density of 16,700 cells/cm^2 using the Lipofectamine RNAiMAX transfection reagent (Life Technologies/Thermo Fisher) per the manufacturer's protocol. Six hours later, the medium was replaced. The lytic cycle was induced two days later. For cGAS and RIG-I knockdowns, the reverse transfection process was done twice, the first time two days prior to induction and a second time on the day of lytic cycle induction. All siRNAs were obtained from Life Technologies/Thermo Fisher.

Realtime quantitative polymerase chain reaction (RT-qPCR)

For RNA analysis, iSLK.219 cells were seeded at a density of 33,000 cells per well in a 24-well plate, and the lytic cycle was induced by the addition of doxycycline (1 μg/ml). RNA

samples were collected at the indicated time points in RNA lysis buffer (Zymo Research). BC3 cells were seeded at 500,000 cells per ml and induced using TPA for 48 h. One ml of the cells was collected, and the cell pellet was lysed in RNA lysis buffer (Zymo Research). Total RNA was extracted using the Quick-RNA MiniPrep kit (Zymo Research) by following the manufacturer's protocol. For mRNA measurements, cDNA was prepared using an iScript cDNA synthesis kit (Bio-Rad) per the manufacturer's protocol. In all cases, 18S rRNA levels were used as an internal standard to calculate relative mRNA levels. Real-time quantitative PCR (RT-qPCR) was performed using iTaq Universal SYBR Green Supermix (Bio-Rad) in a CFX Connect real-time PCR detection system (Bio-Rad). No-template and no-RT controls were included in each replicate. CFX Manager software was used to analyze the data. Primers are listed in Table S3.

Protein analysis

iSLK.219 cells were seeded at a density of 167,000 cells per well in a 6-well plate and treated with doxycycline (1 µg/ml). Lysates were collected at the indicated time points. Cells were lysed in radioimmunoprecipitation assay (RIPA) buffer (50 mM Tris-HCl, pH 7.4, 150 mM NaCl, 2 mM EDTA, 0.5% sodium deoxycholate, 0.1% SDS, 1% NP-40) or an NP-40-only buffer for caspase blots and phospho-protein blots (50 mM Tris-HCl, pH 7.4, 150 mM NaCl, 1 mM EDTA, 0.5% NP-40) supplemented with 50 µg/ml phenylmethylsulfonyl fluoride (PMSF; G-Biosciences) and cOmplete protease cocktail inhibitor (Roche). Samples were separated by SDS-PAGE and transferred to polyvinylidene difluoride (PVDF) membranes. The following Cell

Signaling Technologies antibodies were used on PVDF membranes at 1:1,000 dilution in 5% milk in in Tris-buffered saline with 0.1% Tween 20 (TBST): anti-cGAS (D1D3G) (no. 15102). The following Cell Signaling Technologies antibodies were used with PVDF at 1:1,000 dilution in 5% BSA in TBST: anti-caspase-8 (no. 9746), anti-cleaved caspase-8 (no. 9496), anti-IRF3 (D83B9) (no. 4302), anti-phospho-IRF3 Ser396 (4D4G) (no. 4947), anti-TBK1 (D1B4) (no. 3504), anti-phospho-TBK1 Ser172 (D52C2) (no. 5483), anti-STING (D2P2F) (no. 13647), anti-phospho-STING Ser366 (D7C3S) (no. 19781), anti-RIG-I (D14G6) (no. 3743), anti-NF-κB p65/RelA (D14E12) (no. 8242S), anti-phospho-NF-κB p65 Ser536/RelA (93H1) (no. 3033) and anti-β-tubulin (9F3) (no. 2128). Anti-IFI16 (ab169788; 1:1000, Abcam) and anti-β-actin (ab8229; 1:500, Abcam) were diluted in 5% BSA in TBST and used with PVDF membranes blocked in 5% BSA in TBST. Anti-MAVS (sc-166583, 1:1000 dilution; Santa Cruz Biotechnology) was diluted in 0.5% milk in phosphate-buffered saline with 0.1% Tween 20 (PBST) and used with PVDF membranes blocked in 5% milk in PBST. Horseradish peroxidase (HRP)-conjugated goat anti-rabbit IgG and goat anti-mouse IgG (both 1:5,000 in blocking buffer) were purchased from Southern Biotechnology. HRP-conjugated donkey anti-goat IgG (1:5,000 in 0.5% milk in PBST) was purchased from Santa Cruz Biotechnology. All membranes were exposed using Pierce ECL Western blotting substrate (Thermo Fisher) and imaged with a Syngene G:Box Chemi XT4 gel doc system.

cGAMP ELISA

Cell lysates were harvested 4 days post reactivation in RIPA and subjected to enzyme-linked immunosorbent assay (ELISA) analysis for 2'3'-cGAMP (Cayman Chemical) according to the manufacturers' protocols. Each biological replicate consisted of three technical replicates per condition.

Single cell RNA sequencing

iSLK.219 and iSLK.RTA cells were seeded onto T25 flasks at a density of 16,700 cells/cm^2 and induced with doxycycline in the presence or absence of IDN-6556 (10 μM) and a mixture of neutralizing antibodies against type I IFNs at a 1:500 dilution (39000-1; PBL Assay Science). The media was replaced at day 2 post reactivation with fresh doxycycline, IDN-6556, and type I IFN neutralizing antibodies. Cells were harvested at day 4 post reactivation, washed twice with PBS, and strained to create single cell suspensions at a concentration of 1,000,000/ml. Single cell samples were generated according to 10X Genomics' sample preparation protocol for cultured cell lines (CG00054) and Gel Beads-in-emulsion (GEM) generation protocol (CG000183). Briefly, cells were trypsinized and washed twice with dPBS. Cells were resuspended in dPBS and passed through a 30 μm strainer to remove clumps. Cells were counted and diluted to a concentration of 1,000,000 cells/mL. Cells were mixed with a reverse transcription mastermix (including a primer with polydT anchor) and loaded onto a Chromium B microfluidic chip. Gel beads and partitioning oil were loaded onto the chip and the chip was run through the chromium controller device to generate the GEMs. GEMs were incubated in a

thermal cycler for 1 cycle to generate cDNA. The emulsion was broken, and cDNA was isolated with magnetic beads, amplified for 12 cycles, and then cleaned up with SPRIselect reagent. Libraries were prepared according to 10X Genomics' library construction procol (CG000183). Briefly, cDNA was fragmented and then end-repaired and a-tailed with the enzymes in the provided 10X genomics kit (version 3, PN-1000092). cDNA was double sided size selected using SPRIselect and adaptor oligos were ligated onto the cDNA and further cleaned up with SPRIselect. Paired-end sequencing with 75 cycle read length was performed on an Illumina Nextseq 550 at Tufts Genomics Facility. Raw sequencing data (.bcl files) were processed using the 10X Genomics CellRanger (3.0.0) software. Fastq files were generated for the reads using the mkfastq function as described on the 10X Genomics website (https://support.10xgenomics.com/single-cell-gene-expression/software/pipelines/latest/using/mkfastq). Also using CellRanger, the count function was used to align the reads to a reference genome including the human genome (GRCh38), the KSHV genome (GQ994935.1), and the additional sequence of the RFP/GFP/PAC insertion cassette (Genbank MZ617352). This third reference was added because the GQ994935.1 reference genome corresponds to the KSHV BAC16 genome, whereas our cells contain the rKSHV.219 virus[17,41]. To our knowledge, a full reference for rKSHV.219 is not available. We thus amplified the missing region and sequenced it using Sanger sequencing. The matrix table of gene counts from CellRanger was used as an input for integration and clustering analyses using the R-based Seurat package (version 3.1.1.9021, R version 3.6.1)[20,21]. Cell cycle analysis was done according Tirosh *et al.*[42]. Raw and processed data are available on NCBI GEO, record #

GSE190558. Scripts used for analysis are available on GitHub, https://github.com/mgaglia81/iSLK.219_scRNAseq.

Flow cytometry

iSLK.219-IFNBp-BFP were seeded in 6-well plates at a density of 16,700 cells/cm^2 and induced with doxycycline in the presence or absence of IDN-6556 (10 μM). Four days post infection, cells were trypsinized and fixed with 4% paraformaldehyde. RFP and BFP signals were measured using Becton Dickinson LSRII flow cytometer at the Tufts Laser Cytometry core facility. FlowJo (BD Biosciences) was used to analyze the data.

Statistical analysis

All statistical analysis was performed using GraphPad Prism version 8.4.2 or later (GraphPad Software, La Jolla California USA, www.graphpad.com). Statistical significance was determined by Student's *t*-test or analysis of variance (ANOVA) followed by a *post hoc* multiple comparison test (Dunnett's, Sidak's or Tukey's) when multiple comparisons were required. All data are plotted as mean ± standard deviation.

Acknowledgements

We thank members of the Gaglia laboratory for suggestions and feedback on the project and the manuscript. We thank Drs. Gack, Trono, and Sabatini for sharing reagents. This work was supported by American Cancer Society grant 131320-RSG-17-189-01-MPC to MMG. TT was

supported by the Tufts Collaborative Cancer Biology Award. RCL was supported by NIH training grant T32 GM007310.

References

1. García-Sastre, A. Ten Strategies of Interferon Evasion by Viruses. *Cell Host & Microbe* **22**, 176–184 (2017).
2. White, M. J. *et al.* Apoptotic caspases suppress mtDNA-induced STING-mediated type I IFN production. *Cell* **159**, 1549–1562 (2014).
3. Rongvaux, A. *et al.* Apoptotic caspases prevent the induction of type I interferons by mitochondrial DNA. *Cell* **159**, 1563–1577 (2014).
4. Ning, X. *et al.* Apoptotic Caspases Suppress Type I Interferon Production via the Cleavage of cGAS, MAVS, and IRF3. *Molecular Cell* **74**, 19-31.e7 (2019).
5. Tabtieng, T., Degterev, A. & Gaglia, M. M. Caspase-Dependent Suppression of Type I Interferon Signaling Promotes Kaposi's Sarcoma-Associated Herpesvirus Lytic Replication. *Journal of Virology* **92**, e00078-18 (2018).
6. Cai, X., Chiu, Y.-H. & Chen, Z. J. The cGAS-cGAMP-STING Pathway of Cytosolic DNA Sensing and Signaling. *Molecular Cell* **54**, 289–296 (2014).
7. Wu, J. & Chen, Z. J. Innate immune sensing and signaling of cytosolic nucleic acids. *Annu. Rev. Immunol.* **32**, 461–488 (2014).
8. Schoggins, J. W. Interferon-stimulated genes: roles in viral pathogenesis. *Curr Opin Virol* **6**, 40–46 (2014).
9. Zhang, G. *et al.* Cytoplasmic isoforms of Kaposi sarcoma herpesvirus LANA recruit and antagonize the innate immune DNA sensor cGAS. *PNAS* **113**, E1034–E1043 (2016).

10. Zhang, Y. *et al.* RIG-I Detects Kaposi's Sarcoma-Associated Herpesvirus Transcripts in a RNA Polymerase III-Independent Manner. *mBio* **9**, (2018).
11. Zhao, Y., Ye, X., Dunker, W., Song, Y. & Karijolich, J. RIG-I like receptor sensing of host RNAs facilitates the cell-intrinsic immune response to KSHV infection. *Nat Commun* **9**, 1–14 (2018).
12. Ma, Z. *et al.* Modulation of the cGAS-STING DNA sensing pathway by gammaherpesviruses. *Proc. Natl. Acad. Sci. U.S.A.* **112**, E4306-4315 (2015).
13. Wu, J.-J. *et al.* Inhibition of cGAS DNA Sensing by a Herpesvirus Virion Protein. *Cell Host Microbe* **18**, 333–344 (2015).
14. West, J. A. *et al.* An Important Role for Mitochondrial Antiviral Signaling Protein in the Kaposi's Sarcoma-Associated Herpesvirus Life Cycle. *J. Virol.* **88**, 5778–5787 (2014).
15. Inn, K.-S. *et al.* Inhibition of RIG-I-Mediated Signaling by Kaposi's Sarcoma-Associated Herpesvirus-Encoded Deubiquitinase ORF64. *J. Virol.* **85**, 10899–10904 (2011).
16. Kerur, N. *et al.* IFI16 acts as a nuclear pathogen sensor to induce the inflammasome in response to Kaposi Sarcoma-associated herpesvirus infection. *Cell Host Microbe* **9**, 363–375 (2011).
17. Myoung, J. & Ganem, D. Generation of a doxycycline-inducible KSHV producer cell line of endothelial origin: maintenance of tight latency with efficient reactivation upon induction. *J. Virol. Methods* **174**, 12–21 (2011).
18. Kato, K., Omura, H., Ishitani, R. & Nureki, O. Cyclic GMP-AMP as an Endogenous Second Messenger in Innate Immune Signaling by Cytosolic DNA. *Annu Rev Biochem* **86**, 541–566 (2017).

19. Arvanitakis, L. *et al.* Establishment and characterization of a primary effusion (body cavity-based) lymphoma cell line (BC-3) harboring kaposi's sarcoma-associated herpesvirus (KSHV/HHV-8) in the absence of Epstein-Barr virus. *Blood* **88**, 2648–2654 (1996).
20. Satija, R., Farrell, J. A., Gennert, D., Schier, A. F. & Regev, A. Spatial reconstruction of single-cell gene expression data. *Nature Biotechnology* **33**, 495–502 (2015).
21. Butler, A., Hoffman, P., Smibert, P., Papalexi, E. & Satija, R. Integrating single-cell transcriptomic data across different conditions, technologies, and species. *Nature Biotechnology* **36**, 411–420 (2018).
22. Arias, C. *et al.* KSHV 2.0: a comprehensive annotation of the Kaposi's sarcoma-associated herpesvirus genome using next-generation sequencing reveals novel genomic and functional features. *PLoS Pathog.* **10**, e1003847 (2014).
23. Majerciak, V. *et al.* A Viral Genome Landscape of RNA Polyadenylation from KSHV Latent to Lytic Infection. *PLOS Pathogens* **9**, e1003749 (2013).
24. Jenner, R. G., Albà, M. M., Boshoff, C. & Kellam, P. Kaposi's Sarcoma-Associated Herpesvirus Latent and Lytic Gene Expression as Revealed by DNA Arrays. *J. Virol.* **75**, 891–902 (2001).
25. Lu, M. *et al.* Dissection of the Kaposi's Sarcoma-Associated Herpesvirus Gene Expression Program by Using the Viral DNA Replication Inhibitor Cidofovir. *J. Virol.* **78**, 13637–13652 (2004).
26. Gabaev, I., Williamson, J. C., Crozier, T. W. M., Schulz, T. F. & Lehner, P. J. Quantitative Proteomics Analysis of Lytic KSHV Infection in Human Endothelial Cells Reveals Targets of Viral Immune Modulation. *Cell Reports* **33**, 108249 (2020).

27. Zhao, M., Zhang, J., Phatnani, H., Scheu, S. & Maniatis, T. Stochastic Expression of the Interferon-β Gene. *PLOS Biology* **10**, e1001249 (2012).

28. Eaglesham, J. B. & Kranzusch, P. J. Conserved strategies for pathogen evasion of cGAS-STING immunity. *Curr Opin Immunol* **66**, 27–34 (2020).

29. Bhowmik, D. & Zhu, F. Evasion of Intracellular DNA Sensing by Human Herpesviruses. *Front. Cell. Infect. Microbiol.* **11**, (2021).

30. Hertzog, J. & Rehwinkel, J. Regulation and inhibition of the DNA sensor cGAS. *EMBO reports* **21**, e51345 (2020).

31. Hopfner, K.-P. & Hornung, V. Molecular mechanisms and cellular functions of cGAS–STING signalling. *Nature Reviews Molecular Cell Biology* **21**, 501–521 (2020).

32. Patil, S. *et al.* Single-cell analysis shows that paracrine signaling by first responder cells shapes the interferon-β response to viral infection. *Sci. Signal.* **8**, ra16–ra16 (2015).

33. Rand, U. *et al.* Multi-layered stochasticity and paracrine signal propagation shape the type-I interferon response. *Molecular Systems Biology* **8**, 584 (2012).

34. Fiege, J. K. *et al.* Single cell resolution of SARS-CoV-2 tropism, antiviral responses, and susceptibility to therapies in primary human airway epithelium. *PLOS Pathogens* **17**, e1009292 (2021).

35. Sun, J. *et al.* Single cell heterogeneity in influenza A virus gene expression shapes the innate antiviral response to infection. *PLOS Pathogens* **16**, e1008671 (2020).

36. Kallfass, C., Lienenklaus, S., Weiss, S. & Staeheli, P. Visualizing the Beta Interferon Response in Mice during Infection with Influenza A Viruses Expressing or Lacking Nonstructural Protein 1. *Journal of Virology* **87**, 6925–6930 (2013).

37. Wimmers, F. *et al.* Single-cell analysis reveals that stochasticity and paracrine signaling control interferon-alpha production by plasmacytoid dendritic cells. *Nature Communications* **9**, 3317 (2018).

38. Stürzl, M., Gaus, D., Dirks, W. G., Ganem, D. & Jochmann, R. Kaposi's sarcoma-derived cell line SLK is not of endothelial origin, but is a contaminant from a known renal carcinoma cell line. *International Journal of Cancer* **132**, 1954–1958 (2013).

39. Sancak, Y. *et al.* The Rag GTPases Bind Raptor and Mediate Amino Acid Signaling to mTORC1. *Science* **320**, 1496–1501 (2008).

40. Dull, T. *et al.* A Third-Generation Lentivirus Vector with a Conditional Packaging System. *Journal of Virology* **72**, 8463–8471 (1998).

41. Vieira, J. & O'Hearn, P. M. Use of the red fluorescent protein as a marker of Kaposi's sarcoma-associated herpesvirus lytic gene expression. *Virology* **325**, 225–240 (2004).

42. Tirosh, I. *et al.* Dissecting the multicellular ecosystem of metastatic melanoma by single-cell RNA-seq. *Science* **352**, 189–196 (2016).

43. Jacobs, S. R. *et al.* The Viral Interferon Regulatory Factors of Kaposi's Sarcoma-Associated Herpesvirus Differ in Their Inhibition of Interferon Activation Mediated by Toll-Like Receptor 3. *Journal of Virology* **87**, 798–806 (2013).

44. Yoo, Y.-S. *et al.* The mitochondrial ubiquitin ligase MARCH5 resolves MAVS aggregates during antiviral signalling. *Nat Commun* **6**, 7910 (2015).

45. Gardinassi, L. G., Garcia, G. R., Costa, C. H. N., Silva, V. C. & Santos, I. K. F. de M. Blood Transcriptional Profiling Reveals Immunological Signatures of Distinct States of Infection of Humans with Leishmania infantum. *PLOS Neglected Tropical Diseases* **10**, e0005123 (2016).

46. Rossetto, C. C. & Pari, G. KSHV PAN RNA Associates with Demethylases UTX and JMJD3 to Activate Lytic Replication through a Physical Interaction with the Virus Genome. *PLOS Pathogens* **8**, e1002680 (2012).

Table S1. Characteristics of scRNAseq datasets

	Uninfected + latent	Lytic + vehicle	Lytic + IDN-6556	Lytic + IDN-6556 + anti-IFNS
Total reads	142,704,565	138,925,899	154,624,957	160,218,965
Total cells	5,777	8,310	7,029	9,638
Median reads per cell	22,881	14,739.5	19,083	14,085
Total reads used in analysis	130,047,844	136,742,207	148,241,619	156,671,882
Cells used in analysis	5,406	7,879	6,695	9,159

Table S2. Number and percentage of cells in each cluster

Cluster	Classification	Dataset							
		Uninfected and latent		Lytic + vehicle		Lytic + IDN-6556		Lytic + IDN-6556 + anti-IFNs	
1	uninfected	2365	43.7%	378	4.8%	278	4.2%	251	2.7%
10	latent	16	0.3%	387	4.9%	439	6.6%	420	4.6%
13	latent	185	3.4%	40	0.5%	77	1.2%	79	0.9%
2	latent	1435	26.5%	390	4.9%	429	6.4%	457	5.0%
6	latent (dividing)	255	4.7%	663	8.4%	436	6.5%	437	4.8%
4	latent (dividing)	387	7.2%	942	12.0%	555	8.3%	624	6.8%
3	latent (dividing)	350	6.5%	1004	12.7%	499	7.5%	831	9.1%
0	lytic (early)	3	0.1%	1829	23.2%	1645	24.6%	2416	26.4%
5	lytic (early)	231	4.3%	559	7.1%	517	7.7%	523	5.7%
8	lytic (intermediate)	156	2.9%	667	8.5%	306	4.6%	453	4.9%
7	lytic (intermediate)	2	0.0%	555	7.0%	341	5.1%	693	7.6%
12	lytic (late)	0	0.0%	412	5.2%	274	4.1%	456	5.0%
9	lytic (early) and IFN+	7	0.1%	35	0.4%	385	5.8%	849	9.3%
11	lytic (early) and IFN+	14	0.3%	18	0.2%	514	7.7%	670	7.3%
	total	5406		7879		6695		9159	

Table S3. Primers used for RT-qPCR

Target	*F primer*	*R primer*	*Reference*
Human IFN-β	CAGCAATTTTCAGTGTCAGAAGC	TCATCCTGTCCTTGAGGCAGT	43
Human ISG15	GCGAGATCACCCAGAAGATT	GCCCTTGTTATTCCTCACCA	44
Human IFIT1	GCGCTGGGTATGCGATCTC	CAGCCTGCCTTAGGGGAAG	45
KSHV ORF37	TGACACCCTTGGGTTAACAGT	TCTCGAACCTTGGCGTGCTTTAGA	46

Figure S1

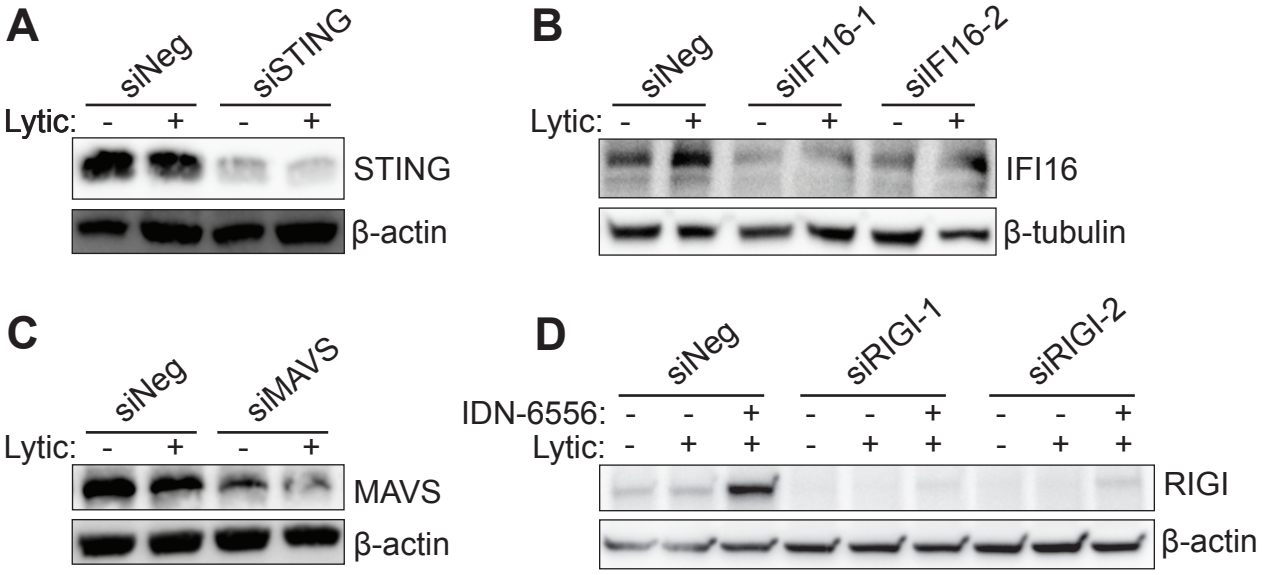

Figure S1. Knockdown of proteins in the type I IFN induction pathway.

iSLK.219 cells were transfected with a negative control siRNA and siRNAs targeting STING (A), IFI16 (B), MAVS (C), or RIG-I (D). Cell lysates were harvested at day 4 post reactivation with doxycycline and treatment with IDN-6556 (where indicared) and subjected to western blotting for the target proteins and β-actin or β-tubulin as loading controls. Blots are representative of 3 replicates.

Figure S2

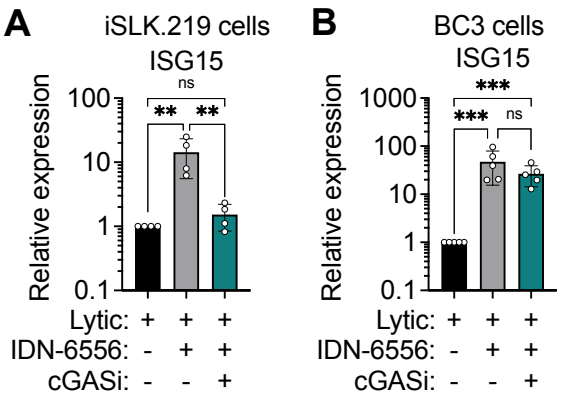

Figure S2. cGAS inhibition counteracts the effects of caspase inhibition on IFN signaling in KSHV-infected cells.

iSLK.219 were lytically reactivated with doxycycline (1 μg/ml) for 3 days and BC3 cells were lytically reactivated with TPA (20 ng/ml) for 2 days. Cells were treated with DMSO (vehicle), IDN-6556 (10 μM), or the cGAS inhibitor RU.521 (cGASi, 24.1 μM) as indicated. Levels of ISG15 and IFIT1 mRNA were measured by RT-qPCR and normalized to 18S rRNA (n = 3). ns, **, ***: *p* value > 0.05, < 0.01, < 0.001, Tukey's multiple comparisons test after two-way ANOVA.

Figure S3

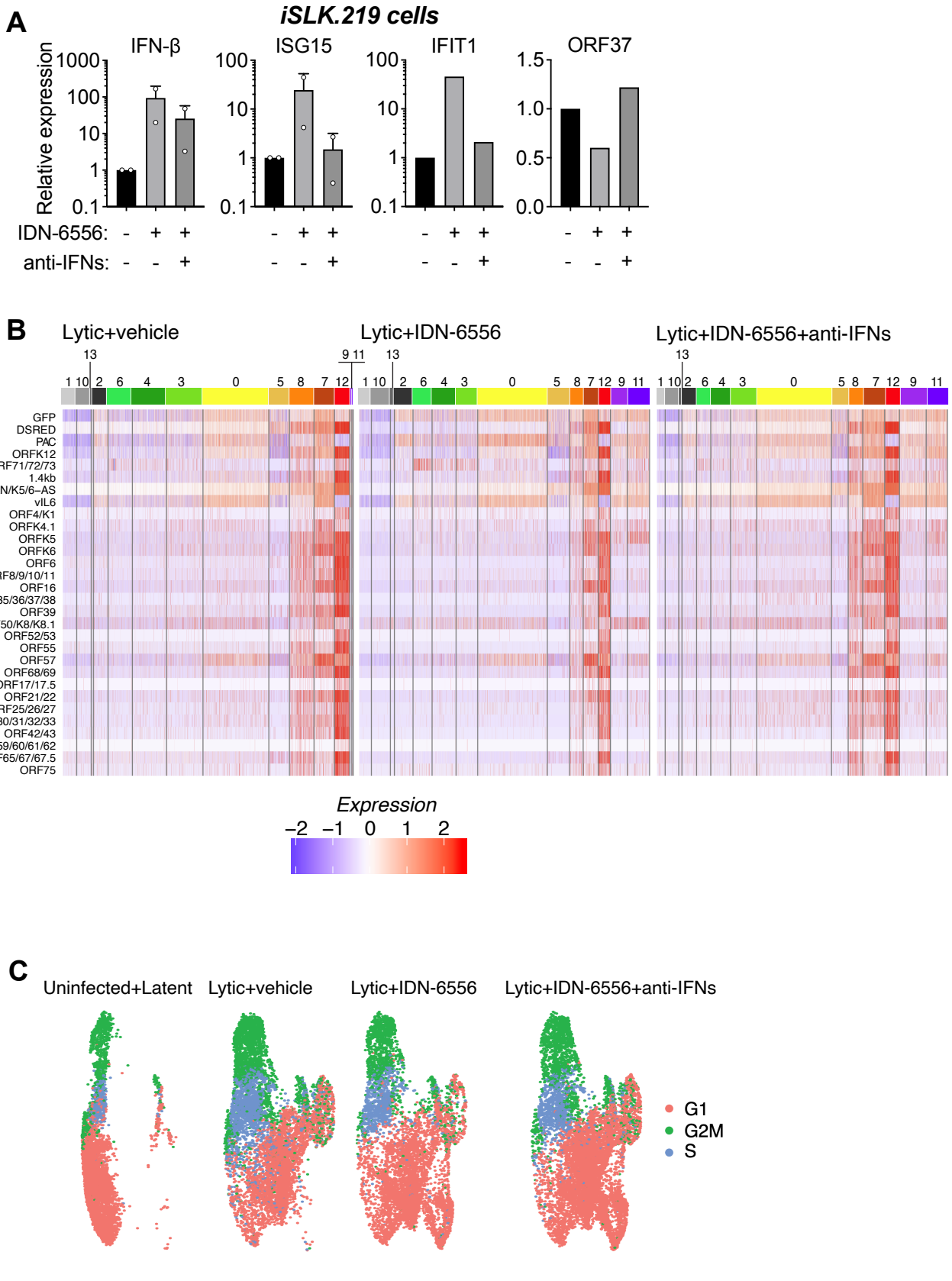

Figure S3. scRNAseq controls and additional analyses. (A) iSLK.219 cells were treated with doxycycline (1 μg/ml) to reactivate the lytic cycle, as well as IDN-6556 and anti-IFN antibodies where indicated. mRNAs levels of IFN- β, the ISGs ISG15 and IFIT1, and the KSHV gene ORF37 were measured by RT-qPCR four days after doxycycline addition. (B-C) Analysis of data from the scRNAseq experiment presented in Figure 3A. (B) Heatmaps of expression of KSHV genes in each cell in the three lytic samples, sorted by cluster. The legend below the heatmaps defines what expression level the colors represent (arbitrary units). (G) UMAP diagram of cell cycle stage classification of cells in the 4 samples.

Figure S4

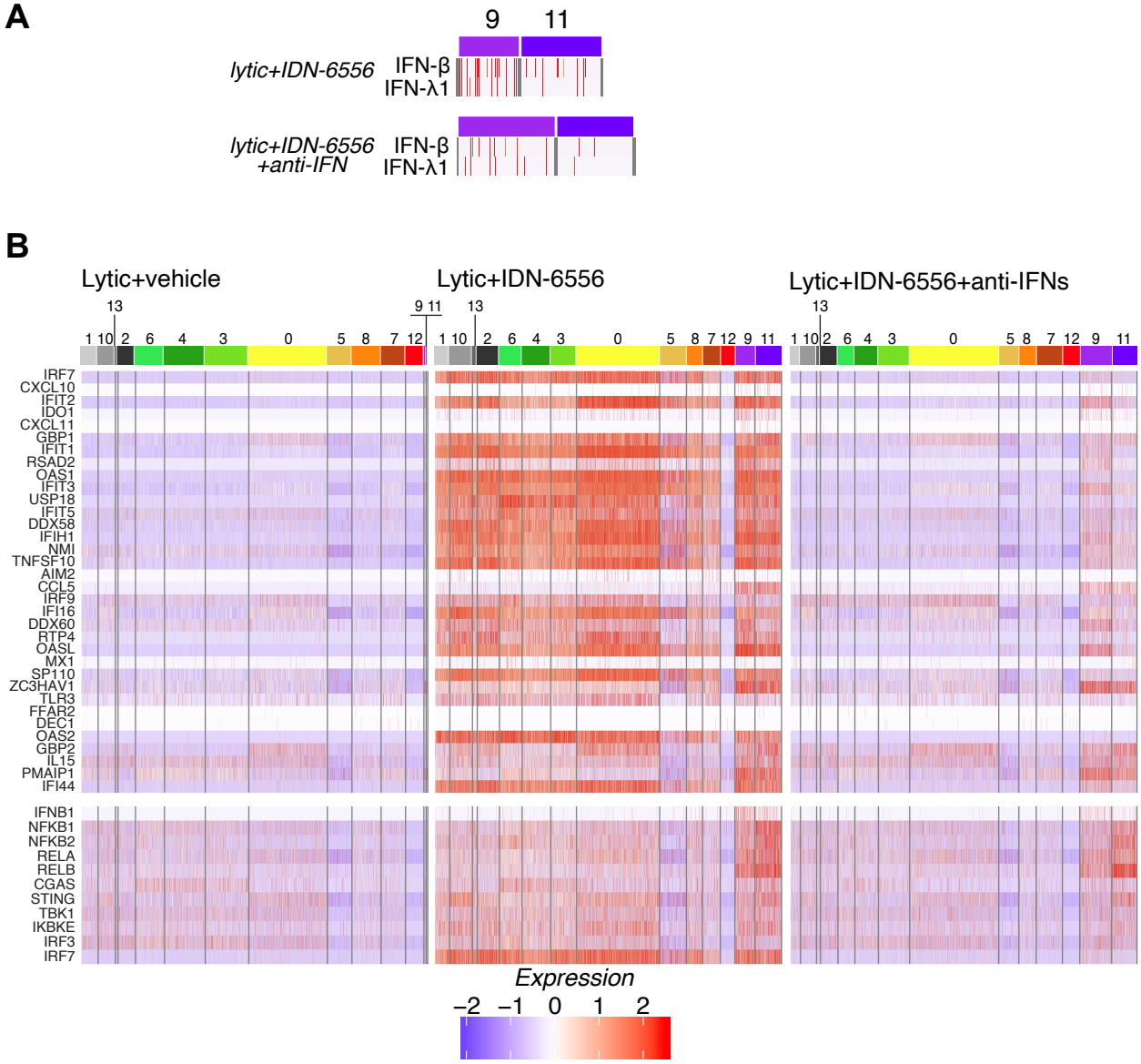

Figure S4. Expression patterns of IFNs, ISGs and genes in the type I IFN induction pathway. Analysis of data from the scRNAseq experiment presented in Figure 3A. (A) Heatmaps of expression of IFN-β and IFN-λ1 in each cell in clusters 9 and 11 in the two IDN-6556 treated samples. (B) Heatmaps of expression of ISGs (top) and select genes from the type I IFN induction pathway (bottom) in each cell in the three lytic samples, sorted by cluster. The legend below the heatmaps defines what expression level the colors represent (arbitrary units).